Design and characterization of LC strain sensors with novel inductor for sensitivity enhancement

2013 Smart Mater. Struct. 22 105015

(http://iopscience.iop.org/0964-1726/22/10/105015)

Smart Mater. Struct. **22** (2013) 105015 (9pp) doi:10.1088/0964-1726/22/10/105015

Design and characterization of LC strain sensors with novel inductor for sensitivity enhancement

Sung-Yueh Wu and Wensyang Hsu

Department of Mechanical Engineering, National Chiao Tung University, 1001 Ta Hsueh Road, Hsinchu 30010, Taiwan

E-mail: whsu@mail.nctu.edu.tw

Received 2 May 2013, in final form 12 August 2013
Published 4 September 2013
Online at stacks.iop.org/SMS/22/105015

Abstract
This paper presents a LC strain sensor with a novel encapsulated serpentine helical inductor. The helical coil of the inductor is formed by serpentine wire to reduce the radial rigidity. Also the inductor is encapsulated by material with high Poisson's ratio. When an axial deformation is applied to this encapsulated inductor, the cross-sectional area of the helical coil will have more evident change due to lower radial rigidity and encapsulation. Therefore, the variation of inductance or LC resonant frequency can be enhanced to provide better sensitivity of the LC strain sensor. By using PDMS as encapsulated material, it is shown that the sensitivity of the conventional helical inductor with or without encapsulation are both about 73.0 kHz/0.01ε, which means that encapsulation on the conventional helical inductor does not help to improve the sensitivity due to high radial rigidity of the conventional helical coil. It is also found that the encapsulated serpentine helical inductor has better sensitivity (121.9 kHz/0.01ε) than the serpentine helical inductor without encapsulation (62.7 kHz/0.01ε), which verifies the sensitivity enhancing capability of the proposed encapsulated serpentine helical inductor design. The error between simulation and measurement results on sensitivity of LC strain sensor with the encapsulated serpentine inductor is about 5.57%, which verifies the accuracy of the simulation model. The wireless sensing capability is also successfully demonstrated.

(Some figures may appear in colour only in the online journal)

1. Introduction

Inductor–capacitor (LC) sensors have attracted much attention due to their capabilities to be wireless and passive. When the inductance L or the capacitance C of the LC circuit is affected by physical or chemical conditions, the resonant frequency f of the LC circuit, listed as equation (1) [1], will change correspondingly. Without battery or other power supply electrically connected to the devices, LC sensors will be suitable for implantable biomedical devices and industrial applications in hazardous environments, which is different from active wireless measurements that need on-board power supply in the sensors [2, 3].

$$f = \frac{1}{2\pi\sqrt{LC}}. \quad (1)$$

For monitoring the resonant frequency of an LC sensor, a network analyzer can be utilized to connect with LC circuits to obtain the frequency response, as shown in figure 1(a). This process can also be performed wirelessly with an antenna connecting to the network analyzer, as shown in figure 1(b).

Applying oscillating voltage to the transmitting antenna, magnetic flux can be generated in nearby space. With inductively coupling the transmitting antenna and the inductor of the LC circuit, forward electromotive forces are induced wirelessly in the inductor based on Faraday's law. Therefore the LC circuit can receive energy by the inductor and store it in the capacitor. With this energy, magnetic flux also can be generated by the LC circuit, and then the backward electromotive forces are induced on the transmitting antenna wirelessly, affecting the charge flow in the antenna. Since both the forward and backward electromotive forces reach a maximum at resonant frequency f of the LC circuit, the frequency response of the antenna changes abruptly at f, and then the resonant frequency can be determined. When

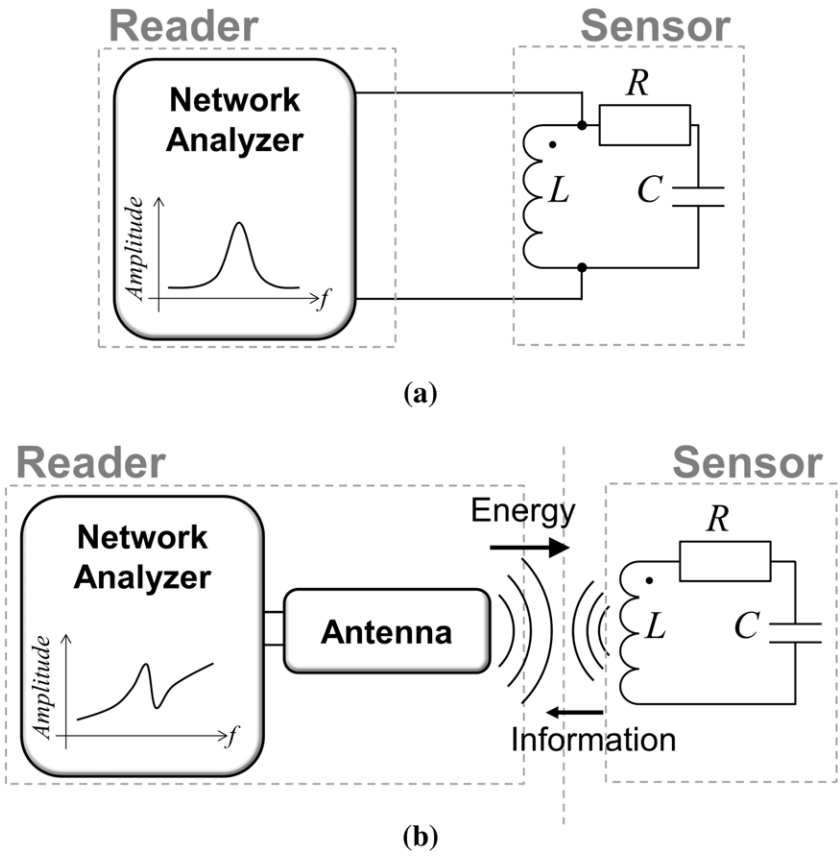

Figure 1. Schematic illustrations of LC sensor: (a) wired; (b) wireless.

the inductance or capacitance is changed by environmental variations, the LC circuit can act as a LC sensor.

Most of the previous LC sensors have been based on the capacitance variations caused by, for example, pressure [1, 4–9], strain [10, 11], humidity [1, 5, 12–14], temperature [1, 12, 15], pH [16], bacteria [17] or specific gases [18]. Only a few designs have utilized the effect from inductance changes, including gap change between two planar inductors [19], a magnetoelastic material [20], cross-sectional area change [21], or position change of a ferrite mass in the inductor [22]. One of the reasons that the inductance is not widely used for sensing is the low sensitivity to the environment. No prior art uses the special geometry of the inductor to enhance the sensitivity.

Here a novel design, an encapsulated serpentine helical inductor, is proposed and shown to enhance the sensitivity of LC sensors for strain sensing. The serpentine design on the inductor can provide lower radial rigidity. With the assistance of proper encapsulation, the sensitivity of LC sensors under axial strain can be enhanced. The effects of both serpentine design and encapsulation are investigated numerically and experimentally. Wireless sensing capability of the proposed inductor design is also examined.

2. Concept design

For a conventional helical inductor, as shown in figure 2(a), the inductance is determined by geometric parameters of the coils and permeability of near space, as listed in equation (2) [23], including axial distributed length l, cross-sectional area A, number of turns N, relative permeability μ_r and permeability of free space μ_0. When the inter-turn spacing is not negligible, a correction factor K needs to be considered. Applying a strain on the conventional helical inductor along the axial direction causes increase of the distributed length l, which will reduce inductance L and increase resonant frequency f. As a result, a helical inductor can work as a strain sensor by monitoring the inductance or resonant frequency variation:

$$L = K\mu_r\mu_0\frac{N^2A}{l}. \tag{2}$$

Smaller cross-sectional area A can also reduce the inductance, as seen in equation (2). To utilize both the distributed length l and cross-sectional area A variations to enhance the sensitivity, a novel encapsulated serpentine helical inductor design is proposed, as shown in figure 2(b). Encapsulating the inductor by proper material with high Poisson's ratio ν, as listed in equation (3) [24], is helpful to enhance the reduction of cross-sectional area while the inductor is under axial loading:

$$\nu = -\frac{\varepsilon_r}{\varepsilon_a}. \tag{3}$$

The Poisson's ratio represents the ability of the material to generate the radial strain ε_r induced by the axial strain ε_a.

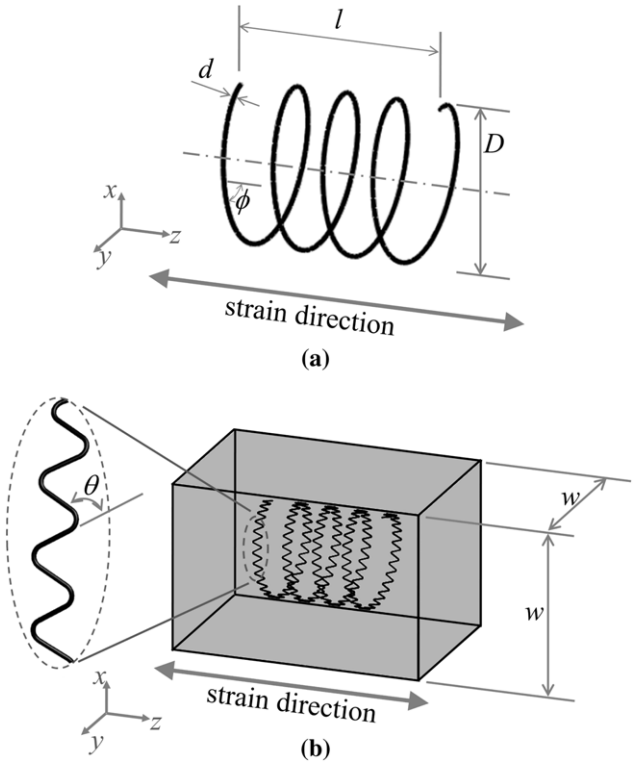

Figure 2. Illustrations of (a) conventional helical inductor; (b) proposed encapsulated serpentine helical inductor.

Compared to the conventional helical coil, the serpentine helical coil can provide lower radial rigidity. When an axial deformation is applied to this encapsulated inductor, the cross-sectional area of the serpentine coil could be further reduced due to the encapsulating material with high Poisson's ratio. Furthermore, encapsulation can protect the inductor from damage or corrosion from the environment. The serpentine angle of the conducting wire is denoted by θ, as shown in figure 2(b). When the serpentine angle is zero, the inductor becomes the conventional helical inductor. The width of the encapsulating material is denoted by w, representing the size of the material utilized to encapsulate the inductor. Therefore, θ and w are two important parameters for serpentine shape and encapsulation designs, respectively. Both increasing distributed length l and decreasing cross-sectional area A can reduce the inductance L and then increase resonant frequency f. A more evident resonant frequency change of LC sensor under the same axial loading means that the LC sensor can provide better sensitivity.

3. Inductor design and analysis

Simulations are performed to find the resonant frequency variation of the proposed encapsulated serpentine helical inductor under different axial strains. Under axial strain ε_a, the distributed length and cross-sectional area are affected, listed as equations (4) and (5) respectively, where l' and l_0 stand for the distributed length with and without applying strain respectively. Similarly, A' and A_0 stand for the cross-sectional

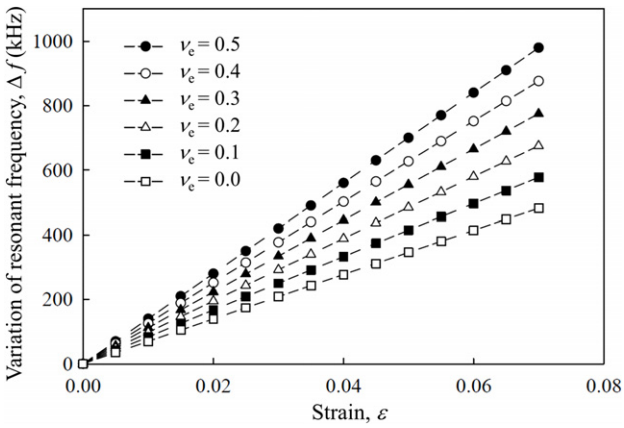

Figure 3. Simulated resonant frequency changes of encapsulated conventional helical inductors with different effective Poisson's ratios. The number of turns N, distributed length l_0, and helical diameter D_0 of the helical coil without applying strain are 36.5, 8 cm, and 1 cm, respectively.

area with and without strain applying respectively. The effective Poisson's ratio ν_e of the inductor, as listed in equation (6), is defined as the ratio between the radial and axial deformations of inductor coils under axial force, whether the inductor is encapsulated or not. The effective Poisson's ratio acts as an important performance index to represent the efficiency on cross-sectional area variation of inductor coil:

$$l' = l_0\,(1 + \varepsilon_a) \tag{4}$$

$$A' = A_0\,(1 - \nu_e \varepsilon_a)^2 \tag{5}$$

$$\nu_e = -\frac{\left(D' - D_0\right) D_0^{-1}}{\left(l' - l_0\right) l_0^{-1}}, \tag{6}$$

where D' and D_0 stand for the diameters of the helical coil with and without applying strain, respectively. By combining equations (2), (4), (5) and (6), the inductance becomes

$$L' = K' \mu_r \mu_0 \frac{N^2 A'}{l'} = \frac{K'}{K_0} \frac{(1 - \nu_e \varepsilon_a)^2}{(1 + \varepsilon_a)} L_0, \tag{7}$$

where K' and K_0 stand for the correction factor with and without applying strain respectively. Similarly, L' and L_0 stand for the inductance with and without applying strain respectively. It can be found from equations (1) and (7) that applying tensile strain ($\varepsilon_a > 0$) leads to smaller inductance and higher resonant frequency, and this effect can be further enhanced with high effective Poisson's ratio, as shown in figure 3. Since the encapsulating material with high Poisson's ratio is helpful to increase the effective Poisson's ratio of the inductor, polydimethylsiloxane (PDMS), a polymer with good transparency and biocompatibility [25], is chosen here as the encapsulating material for its high Poisson's ratio of 0.5 [26].

A capacitor 15 pF which is small enough for high quality factor is selected to connect with the inductor for simulations and experiments. Figure 4 shows how the geometric parameters of the inductor affect the initial inductance and resonant frequency sensitivity with initial distributed length 80 mm and effective Poisson's ratio 0.5. The

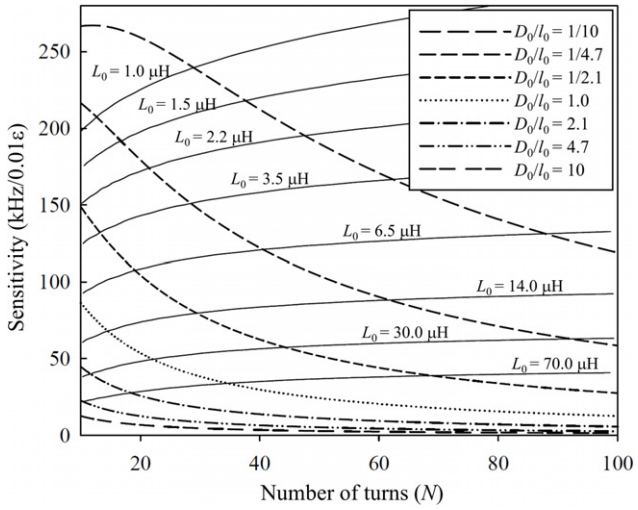

Figure 4. Simulated sensitivity with effective Poisson's ratio 0.5 and different helical inductor dimensions.

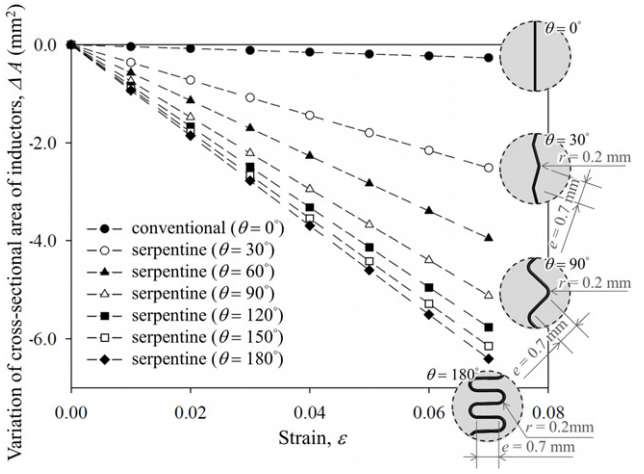

Figure 5. Simulated cross-sectional area variations of the encapsulated inductor with encapsulation width $w = 20$ mm by ANSYS. The number of turns N, distributed length l_0, helical diameter D_0, and coil diameter d of the helical coil without applying strain are 36.5, 8 cm, 1 cm, and 0.1 mm, respectively.

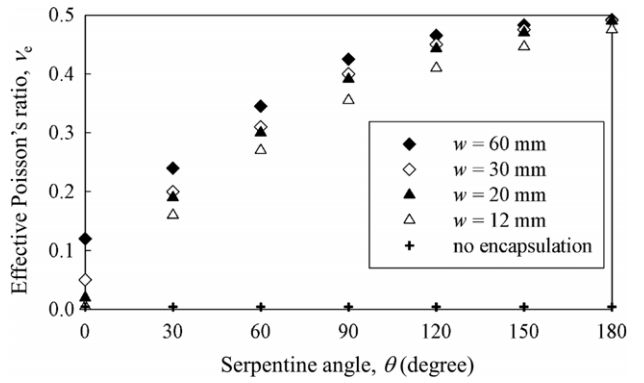

Figure 6. Simulated results of the effective Poisson's ratios at various serpentine angles θ and encapsulation width w. The number of turns N, distributed length l_0, helical diameter D_0, and coil diameter d of the helical coil without applying strain are 36.5, 8 cm, 10 mm, and 0.1 mm, respectively.

sensitivity, which is defined as the variation of the resonant frequency per 0.01 axial strain, can be obtained through equations (1) and (7). It is found that smaller diameter–length ratio D/l and fewer coil numbers N can provide higher sensitivity, but that may result in low initial inductance L_0 as well as low quality factor, which is not helpful for wireless resonant frequency monitoring. Here we select initial inductance 2.2 μH, number of turns 36.5, diameter–length ratio 1/8 and wire diameter 0.1 mm as an example for the following simulations and experiments. The number of turns is not an integer due to the need for smooth connection between the inductor and capacitor.

For the coils without encapsulation, the effective Poisson's ratio mainly depends on the geometric dimensions, as listed in equation (8), which can be derived from equation (6) and basic trigonometry. S stands for the invariable wire length while axial strain is applied. ϕ_0 stands for the helix angle before strain is applied:

$$\nu_{\text{e, no encap.}} = \frac{S\Delta\phi\cos(\phi_0)\cdot(N\cdot\pi\cdot D_0)^{-1}}{S\cdot\Delta\phi\cdot\sin(\phi_0)\cdot(l_0)^{-1}} = \frac{l_0\cot(\phi_0)}{N\pi D_0}. \quad (8)$$

However, for the coil with encapsulation, the radial deformation cannot be derived similarly due to the complicated composite structure. Although the coil is encapsulated by material with high Poisson's ratio, the effective Poisson's ratio of the inductor will not be the same as the Poisson's ratio of the encapsulating material due to the radial rigidity of the encapsulated coil. Therefore, further numerical simulations are performed by commercial finite element method (FEM) software, ANSYS Workbench, with copper as the coil material encapsulated by PDMS under different axial strains. Variations of coil cross-sectional area with different serpentine angles θ and widths w of encapsulating material are investigated. Figure 5 shows simulated cross-sectional area variations of the conventional and the proposed serpentine helical coils with different serpentine angles under encapsulation. Detailed dimensions of the serpentine wire are also shown in figure 5, such as serpentine curvature radius r and elongating length e. It is found that the cross-sectional area variation rate of encapsulated conventional helical coils ($\theta = 0°$) is -0.038 mm^2/0.01ε. For the encapsulated serpentine helical coils, the cross-sectional area variation rate can be enhanced from -0.359 mm^2/0.01ε ($\theta = 30°$) to -0.915 mm^2/0.01ε ($\theta = 180°$), indicating that lower radial rigidity and larger cross-sectional area variation can be achieved through serpentine design with encapsulation.

The effective Poisson's ratio of encapsulated inductors, as shown in figure 6, can be calculated by equation (6) based on the simulated cross-sectional area variation results in figure 5. It is found that the effective Poisson's ratio becomes higher with a larger serpentine angle and then reaches a saturated value around 0.5, which is the Poisson's ratio of the encapsulating material. As a result,

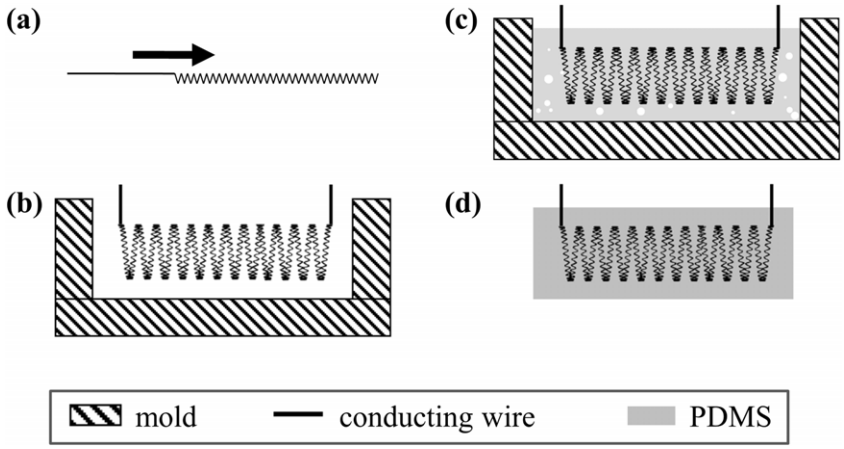

Figure 7. Fabrication process of the encapsulated serpentine helical inductor.

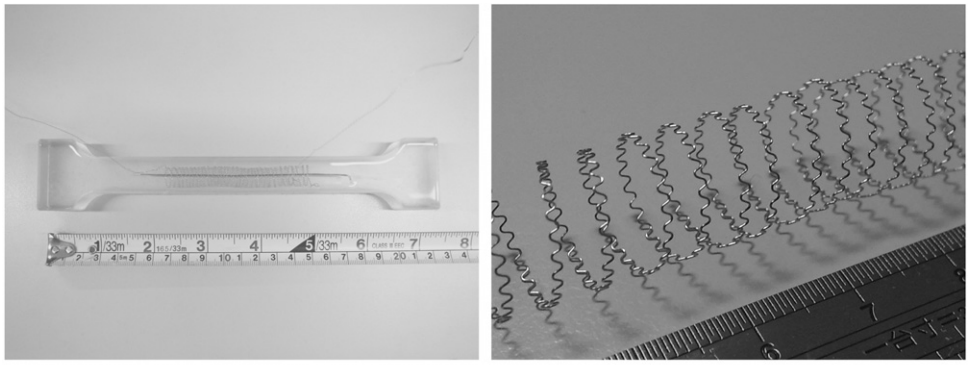

Figure 8. Photos: (a) encapsulated serpentine helical inductor, (b) close view of the serpentine helical inductor before the encapsulation.

the Poisson's ratio of the encapsulating material can be considered as the upper bound of the effective Poisson's ratio of the encapsulated inductor. For the inductors without encapsulation at the same dimensions ($l_0 = 80$ mm, $N = 36.5$, $D_0 = 10$ mm, $\phi_0 = 86.01°$), the effective Poisson's ratio calculated by equation (8) is only 0.004 in all serpentine angle range, as shown in figure 6. It indicates that encapsulation is a critical factor in sensitivity enhancement.

The size of encapsulating material is also shown to affect the effective Poisson's ratio of the inductor. As shown in figure 6, a wider encapsulating material width w leads to a higher effective Poisson's ratio. For the conventional helical inductor ($\theta = 0°$) with encapsulating width $w = 60$ mm, which is six times the inductor diameter, the effective Poisson's can be enhanced from 0.004 to 0.12. For the serpentine inductor with $\theta = 30°$ and $w = 60$ mm, the effective Poisson's ratio can be enhanced to 0.24, which can be further increased through larger θ. However, when serpentine angle is larger than 90°, the enhancements for encapsulation width $w = 20$, 30, and 60 mm are very close. Therefore, 20 mm on encapsulation width is chosen for later experiments.

Once the radial deformation of the inductor with or without encapsulation is obtained from FEM simulations or basic trigonometry, the resonant frequency variation can be simulated by equations (1) and (2). For the serpentine helical inductor with special zigzag shape, the line integral method [27] to simulate an arbitrarily-wound shape inductor is also used here for more accurate inductance calculation.

4. Fabrication and testing

The fabrication process of the proposed encapsulated serpentine helical inductor is shown in figure 7. First, the round copper wire is processed to form serpentine wire by an in-house machine which is made from two spur gears driven by a DC motor. The round wire is drawn in by the continuous rotation of two spur gears to obtain a serpentine shape. Then the serpentine wire is wound to become helical coils to form the serpentine helical inductor. The inductor is then placed in a mold and encapsulated by liquid PDMS. After 15 min pumping to remove the bubbles in the encapsulating material, PDMS, the whole mold is placed in a hot oven at 80 °C for 150 min to solidify the PDMS. After removing the mold, the encapsulated serpentine helical inductor is obtained.

The fabricated encapsulated serpentine helical inductor is shown in figure 8, with number of turns $N = 36.5$, distributed length $l = 83$ mm, inductor diameter $D_0 = 11$ mm, helix angle $\phi_0 = 86.2°$, wire diameter $d_0 = 0.1$ mm, encapsulating width $w = 20$ mm, serpentine angle $\theta = 120°$, serpentine radius

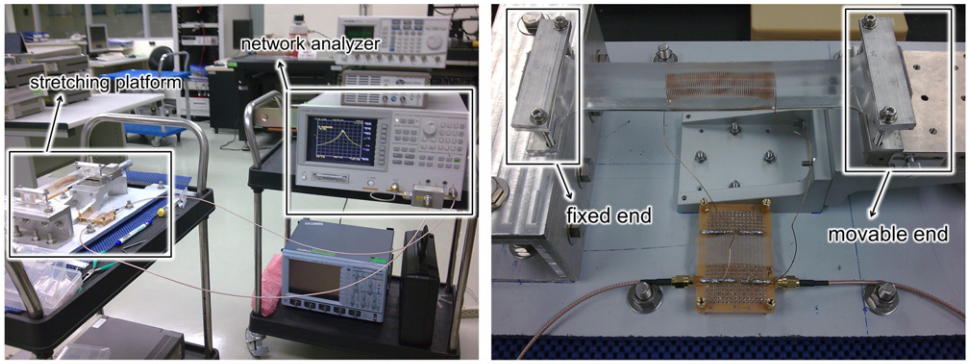

Figure 9. Photos of measurement setup: (a) stretching platform and network analyzer, (b) close view of the stretching platform.

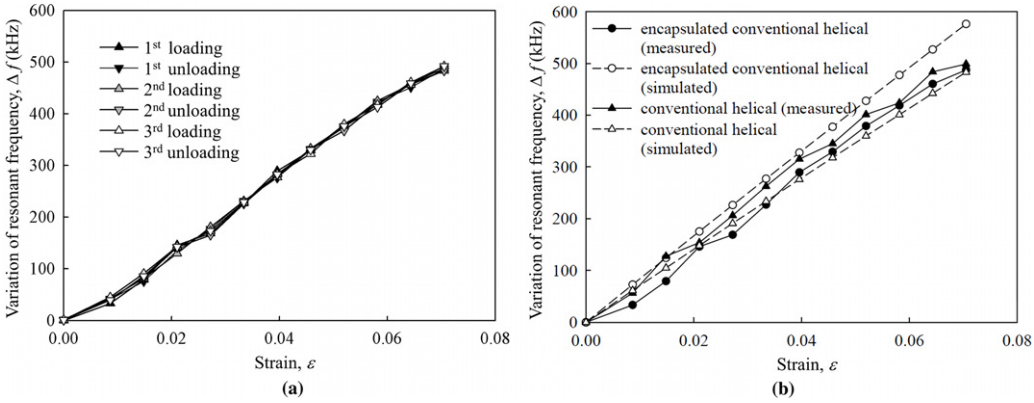

Figure 10. Results: (a) measured resonant frequency variations of the encapsulated conventional helical inductor ($\theta = 0°$) with three loading/unloading cycles. (b) Measured and simulated resonant frequency variations of the conventional helical inductors ($\theta = 0°$) with or without encapsulation.

curvature $r = 0.2$ mm, and elongating length $e = 0.7$ mm. Since the serpentine shape is formed by the rotation of two spur gears, the serpentine angle is decided by the shape of the gear teeth. With gears having sharper teeth, larger serpentine angle can be obtained. Encapsulated conventional helical inductors with similar dimensions are also fabricated for performance comparison.

The resonant frequency of the LC circuit is measured by the network analyzer (Agilent 4395A), as shown in figure 9(a). Strain is applied manually through the stretching platform, as shown in figure 9(b), where one end of the strain sensor is fixed and the other end is clamped to a movable stage MISUMI ZSG80. The strain is controlled by manually adjusting the movable stage to stretch the strain sensor. Due to the good transparency of the encapsulating material, the axial length variations of the encapsulated inductor can be measured by a vernier caliper with resolution 0.05 mm. At first, we gradually stretch the inductor to cause an axial extension of 0.5 mm in about one minute, which is about 0.6% ε, and then the resonant frequency of the strain sensor is measured. Then we stretch the inductor for another 0.5 mm in about one minute to make another frequency measurement. The process is repeated several times until the strain reaches about 7%, and then the strain sensor is unloaded with frequency measurement in a similar manner.

5. Results and discussion

Table 1 shows the measured and simulated resonant frequencies of LC circuits with conventional and serpentine helical inductors having similar helical dimensions before applying axial strain, where the capacitance is 15.0 ± 5% pF. Inductance simulations based on both equation (2) and the line integral method are performed. It is found that both methods have good agreement with the experimental data for the LC circuit with conventional inductor, where errors are around 2.57%–3.21%. But for the LC circuit with serpentine helical inductor, equation (2) leads to an error of about 9.24%, which is reduced to 3.49% by using the line integral method. Therefore, simulations of resonant frequency are based on equation (1) and the line integral method in the following calculations for the serpentine inductor.

Figure 10(a) shows the measurement results of three loading/unloading tests of the encapsulated conventional helical inductors ($\theta = 0°$). Figure 10(b) shows the measured and simulated resonant frequency changes of conventional helical inductors ($\theta = 0°$) with and without encapsulation. The simulated effective Poisson's ratios of the conventional helical inductor with and without encapsulation are 0.02 and 0.004, respectively. It is found that the sensitivity of both inductors is about 73.0 kHz/0.01ε, and the encapsulation on

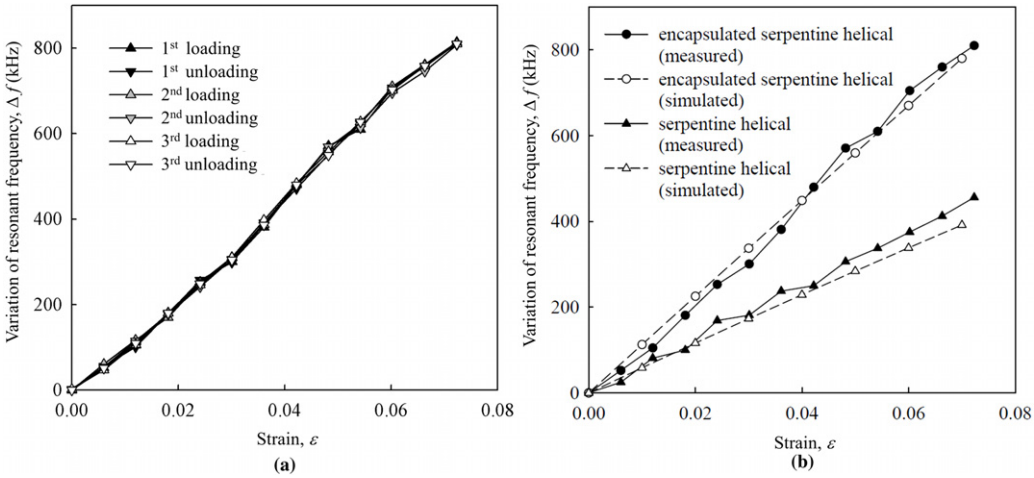

Figure 11. Results: (a) measured resonant frequency variations of the proposed encapsulated serpentine ($\theta = 120°$) helical inductor with three loading/unloading cycles; (b) measured and simulated resonant frequency variations of the proposed serpentine helical inductors ($\theta = 120°$) with or without encapsulation.

Table 1. Measured and simulated resonant frequencies of LC circuits with the conventional helical ($\theta = 0°$) and serpentine helical ($\theta = 120°$) inductors before applying axial strain.

		Measured	Simulation by equations (1) and (2)		Simulation by equation (1) and line integral method	
Inductor type	Capacitor (pF)	f (MHz)	f (MHz)	Error (%)	f (MHz)	Error (%)
Conventional	15.0 (±5%)	23.35	24.10	3.21	23.95	2.57
Serpentine	15.0 (±5%)	22.06	24.10	9.24	22.83	3.49

the conventional helical inductor does not help to improve the sensitivity. This is due to the high radial rigidity of the conventional helical coils, which resists the radial compression from encapsulating material during axial strain application.

Three loading/unloading tests of the proposed encapsulated serpentine helical inductors ($\theta = 120°$) are also performed, and the results are shown in figure 11(a). Figure 11(b) shows the measured and simulated resonant frequency changes of the serpentine helical inductor with and without encapsulation. The simulated effective Poisson's ratios of the serpentine helical inductors with and without encapsulation are 0.443 and 0.004, respectively. The measured results show that the encapsulated serpentine helical inductor has better sensitivity (121.9 kHz/0.01ε) than the serpentine helical inductor without encapsulation (62.7 kHz/0.01ε), verifying the sensitivity enhancing capability of the proposed encapsulated serpentine helical design. The error between simulation and measurement results on sensitivity of LC circuit with encapsulated serpentine inductor is about 5.57%, which verifies the accuracy of the simulation model.

The capability of the wireless sensing of the proposed serpentine inductor design is also tested. Wireless measurement of the resonant frequency is achieved by the network analyzer connecting to the two-antenna setup [5]. Wireless measurement results of three loading/unloading tests of the proposed encapsulated serpentine helical inductors ($\theta = 120°$) are shown in figure 12(a). Figure 12(b) shows the wireless measurement results of the conventional and serpentine helical inductors with and without encapsulation for 5 cm wireless sensing distance. It shows that the sensitivities of conventional helical inductors with or without encapsulation are both around 70.1 kHz/0.01ε, and the encapsulated serpentine helical inductor has better sensitivity (119.7 kHz/0.01ε) than the serpentine helical inductor without encapsulation (59.7 kHz/0.01ε). There is about 5% difference between the wireless and wired measured sensitivities, which could be further reduced through higher quality factor of the LC circuit [28].

6. Conclusions

Here an encapsulated serpentine helical inductor is proposed, designed, fabricated and tested to enhance the sensitivity of LC sensors. When an axial deformation is applied to this encapsulated inductor, the cross-sectional area of the helical coil is shown to have more evident change than the conventional helical inductor due to lower radial rigidity and encapsulation. It is found that the sensitivity of conventional helical inductor with or without encapsulation is in both cases about 73.0 kHz/0.01ε, which means that encapsulation on the conventional helical inductor does not help to improve the sensitivity due to the high radial rigidity of the conventional helical coil. It is also found that the encapsulated serpentine helical inductor has better sensitivity (121.9 kHz/0.01ε) than the serpentine helical inductor without encapsulation

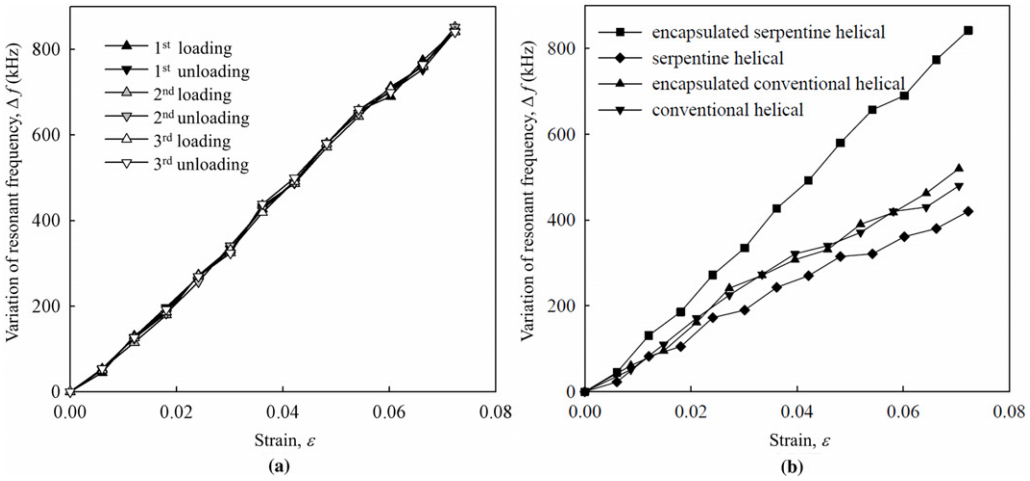

Figure 12. Wireless measured resonant frequency variations of: (a) the proposed encapsulated serpentine ($\theta = 120°$) helical inductor with three loading/unloading cycles; (b) the proposed serpentine ($\theta = 120°$) helical inductor and the conventional ($\theta = 0°$) helical inductors with or without encapsulation.

(62.7 kHz/0.01ε). The proposed inductor design can be combined with other techniques based on capacitance variation to further enhance the sensitivity of LC sensors.

Acknowledgments

This work was supported by the National Science Council of Taiwan under Grant NSC 101-2625-M009-008. Authors would also like to thank the National Chip Implementation Center of Taiwan for providing the measurement facilities.

References

[1] Ong K G, Grimes C A, Robbins C L and Singh R S 2001 Design and application of a wireless, passive, resonant-circuit environmental monitoring sensor *Sensors Actuators* A **93** 33–43

[2] Leung A M, Ko W H, Spear T M and Bettice J A 1986 Intracranial pressure telemetry system using semicustom integrated circuits *IEEE Trans. Biomed. Eng.* **33** 386–95

[3] Todoroki A, Miyatani S and Shimamura Y 2003 Wireless strain monitoring using electrical capacitance change of tire: part I—with oscillating circuit *Smart Mater. Struct.* **12** 403–9

[4] Shin K H, Moon C R, Lee T H, Lim C H and Kim Y J 2005 Flexible wireless pressure sensor module *Sensors Actuators* A **123/124** 30–5

[5] Ong K G and Grimes C A 2000 A resonant printed-circuit sensor for remote query monitoring of environmental parameters *Smart Mater. Struct.* **9** 421–8

[6] Rosengren L, Bäcklund Y, Sjöström T, Hök B and Svedbergh B 1992 A system for wireless intra-ocular pressure measurements using a silicon micromachined sensor *J. Micromech. Microeng.* **2** 202–4

[7] Akar O, Akin T and Najafi K 2001 A wireless batch sealed absolute capacitive pressure sensor *Sensors Actuators* A **95** 29–38

[8] Fonseca M A, English J M, Arx M v and Allen M G 2002 Wireless micromachined ceramic pressure sensor for high-temperature applications *J. Microelectromech. Syst.* **11** 337–43

[9] Chen P-J, Rodger D C, Saati S, Humayun M S and Tai Y-C 2008 Microfabricated implantable parylene-based wireless passive intraocular pressure sensors *J. Microelectromech. Syst.* **17** 1342–51

[10] Jia Y, Sun K, Agosto F J and Quiñones M T 2006 Design and characterization of a passive wireless strain sensor *Meas. Sci. Technol.* **17** 2869–76

[11] Matsuzaki R and Todoroki A 2005 Passive wireless strain monitoring of tyres using capacitance and tuning frequency changes *Smart Mater. Struct.* **14** 561–8

[12] DeHennis A D and Wise K D 2005 A wireless microsystem for the remote sensing of pressure, temperature, and relative humidity *J. Microelectromech. Syst.* **14** 12–22

[13] Harpster T J, Hauvespre S, Dokmeci M R and Najafi K 2002 A passive humidity monitoring system for *in situ* remote wireless testing of micropackages *J. Microelectromech. Syst.* **11** 61–7

[14] Ong J B, You Z, Mills-Beale J, Tan E L, Pereles B D and Ong K G 2008 A wireless, passive embedded sensor for real-time monitoring of water content in civil engineering materials *IEEE Sensors J.* **8** 2053–8

[15] Marioli D, Sardini E and Serpelloni M 2010 Passive hybrid MEMS for high-temperature telemetric measurements *IEEE Trans. Instrum. Meas.* **59** 1353–61

[16] García-Cantón J, Merlos A and Baldi A 2007 A wireless LC chemical sensor based on a high quality factor EIS capacitor *Sensors Actuators* B **126** 648–54

[17] Ong K G, Bitler J S, Grimes C A, Puckett L G and Bachas L G 2002 Remote query resonant-circuit sensors for monitoring of bacteria growth: application to food quality control *Sensors* **2** 219–32

[18] Ong K G, Zeng K and Grimes C A 2002 A wireless, passive carbon nanotube-based gas sensor *IEEE Sensors J.* **2** 82–8

[19] Sridhar V and Takahata K 2008 A hydrogel-based wireless sensor using micromachined variable inductors with folded flex-circuit structures for biomedical applications *Proc. IEEE Int. Conf. on Micro Electro Mechanical Systems 2008 (Tucson, AZ)* pp 70–3

[20] Ludwig A, Frommberger M, Tewes M and Quandt E 2003 High-frequency magnetoelastic multilayer thin films and applications *IEEE Trans. Magn.* **39** 3062–7

[21] Butler J C, Vigliotti A J, Verdi F W and Walsh S M 2002 Wireless, passive, resonant-circuit, inductively coupled, inductive strain sensor *Sensors Actuators* A **102** 61–6

[22] Baldi A, Choi W and Ziaie B 2003 A self-resonance frequency-modulated micromachined passive pressure transensor *IEEE Sensors J.* **3** 728–33
[23] Welsby V G 1960 *The Theory and Design of Inductance Coils* (London: MacDonald & Co.)
[24] Craig R R Jr 2001 *Mechanics of Materials* 2nd edn (New York: Wiley)
[25] Tsai N-C and Sue C-Y 2007 Review of MEMS-based drug delivery and dosing systems *Sensors Actuators* A **134** 555–64
[26] Mark J E 1999 *Polymer Data Handbook* (New York, NY: Oxford University Press)
[27] Sijoy C D and Chaturvedi S 2005 Fast and accurate inductance calculations for arbitrarily-wound coils for pulsed power applications *Proc. IEEE Conf. on Pulsed Power 2005 (Monterey, CA)* pp 1464–7
[28] Nopper R, Niekrawietz R and Reindl L 2010 Wireless readout of passive LC sensors *IEEE Trans. Instrum. Meas.* **59** 2450–7